

Cite this: *Metallomics*, 2011, **3**, 28–37

www.rsc.org/metallomics

CRITICAL REVIEW

Trace metal imaging with high spatial resolution: Applications in biomedicine

Zhenyu Qin,^{*ac} Joseph A. Caruso,^b Barry Lai,^d Andreas Matusch^e and J. Sabine Becker^f

Received 14th September 2010, Accepted 4th November 2010

DOI: 10.1039/c0mt00048c

New generations of analytical techniques for imaging of metals are pushing hitherto boundaries of spatial resolution and quantitative analysis in biology. Because of this, the application of these imaging techniques described herein to the study of the organization and dynamics of metal cations and metal-containing biomolecules in biological cell and tissue is becoming an important issue in biomedical research. In the current review, three common metal imaging techniques in biomedical research are introduced, including synchrotron X-ray fluorescence (SXRF) microscopy, secondary ion mass spectrometry (SIMS), and laser ablation inductively coupled plasma mass spectrometry (LA-ICP-MS). These are exemplified by a demonstration of the dopamine-Fe complexes, by assessment of boron distribution in a boron neutron capture therapy cell model, by mapping Cu and Zn in human brain cancer and a rat brain tumor model, and by the analysis

^a Department of Medicine, College of Medicine, University of Cincinnati, Cincinnati, OH 45267, USA

^b Department of Chemistry, College of Arts and Sciences, University of Cincinnati, Cincinnati, OH 45267, USA

^c Department of Surgery, Vascular Surgery Division, University of Texas Health Science Center at San Antonio, San Antonio, TX 78229, USA. E-mail: qinz@uthscsa.edu; Fax: (210) 567-1762; Tel: (210) 567-5715

^d X-Ray Science Division, Argonne National Laboratory, Argonne, Illinois 60439, USA

^e Institute of Neurosciences and Medicine, Forschungszentrum Juelich, D-52425, Juelich, Germany

^f Central Division of Analytical Chemistry, Forschungszentrum Juelich, D-52425, Juelich, Germany. Web: (www.brainmet.com)



Zhenyu Qin

Dr Zhenyu Qin is a vascular biologist and a director of the Vascular Metallomics Research Laboratory of the Division of Vascular Surgery, University of Texas Health Science Center at San Antonio. His research interest focuses on the vascular function of metals (with a particular emphasis on copper and ATP7A) at physiological and pathological levels. Trace metal bioimaging is a natural extension of his research field.



Joseph A. Caruso

Dr Caruso holds a PhD from Michigan State University. After a postdoctoral fellowship at The University of Texas - Austin, he joined the University of Cincinnati Chemistry faculty and since then he has authored or co-authored 380 scientific publications and presented more than 325 invited lectures. His current research interests are in metallomics studies in biomedical research areas. Caruso is a member of the Society for Applied Spectroscopy and a Fellow of the Royal

Society of Chemistry. He is Chair of the RSC Metallomics editorial board. He has been honored many times—his most recent award was to be elected Fellow of the Society of Applied Spectroscopy.

of metal topography within neuromelanin. These studies have provided solid evidence that demonstrates that the sensitivity, spatial resolution, specificity, and quantification ability of metal imaging techniques is suitable and highly desirable for biomedical research. Moreover, these novel studies on the nanometre scale (*e.g.*, of individual single cells or cell organelles) will lead to a better understanding of metal processes in cells and tissues.

1. Introduction

Metals are vital components of chemistry and life.¹ An estimated one-third of all proteins require metal ions as cofactors for protein function.² Indeed, the homeostasis of metal ions [*e.g.*, iron (Fe), copper (Cu), zinc (Zn), manganese (Mn), potassium (K), sodium (Na), and calcium (Ca)] is essential for many biological activities.³ The surplus or deficit of these elements may lead to various human diseases. For example, human Menkes disease is a genetic disorder of Cu metabolism caused by mutations of ATP7A. A lack of this protein results in progressive neurodegeneration and vascular tissue abnormalities; death by 3 years of age is typical.⁴ In many neurodegenerative diseases, metal-containing deposits

(such as those found in Wilson's, Parkinson's, and Alzheimer's disease) or metal deficiencies (such as the lack of copper in Menkes disease; mutations of Menkes disease gene coding for ATP7A that is responsible for excretion of copper from cells and delivery of this cofactor to copper containing enzymes such as SOD3 in the trans-Golgi apparatus⁵) were observed within the brain. Therefore, the functions of metal ions in cellular regulation and signaling as they apply to the healthy or disease states, are of principal interest in biomedicine.

From a chemical standpoint, the inventory of metals and their species in cells and tissues (including metalloproteins and/or metalloenzymes) is termed as the metallome and the analysis thereof metallomics.⁶ From a biomedical standpoint, metallomics investigates how the metals are bound to biomolecules, characterizes metalloproteins and/or metalloenzymes and studies the mechanisms of enzymatic and biochemical reactions, and provides a novel perspective to investigate the pathophysiological mechanism of diseases. Metallomics will also help to better understand the basic cellular nutritional requirements for essential metals. It is anticipated that the use of metallomics will also contribute to new drug design, diagnostics, and therapeutics involving metal complexes. Moreover, extending the concept of metallomics into biomedical research has resulted in new research subjects. As a useful example, vascular metallomics, a branch of vascular biology, is emerging.⁷ This methodology is used to study the biological role of metal ions and their signaling pathways in the vasculature, using techniques including molecular biology, cell biology, genetics, and analytical chemistry.

In general, all essential, beneficial, and toxic metals are not homogeneously distributed in biological cells and tissues. Thus, more fruitful insights into physiology and



Barry Lai

Dr Barry Lai received his PhD Degree in physics from the University of Wisconsin-Madison. He then joined the Advanced Photon Source at Argonne National Laboratory as postdoctoral fellow and later as staff physicist. He worked on synchrotron X-ray optics and development of X-ray microscopy techniques. His current interests focus on developing next generation X-ray fluorescence nano-probes and exploring their applications in life, materials, and environmental science.



Andreas Matusch

Dr Andreas Matusch studied medicine and physics at the universities of Marburg, Munich, Poitiers and Paris-VI. After obtaining his MD in medicine 2000 he received clinical education in Neurology in Paris and since 2003 he has worked at the Research Center Jülich in the field of molecular neuroimaging using mass spectrometric and radiotracer techniques at the junction of medicine, analytical and nuclear chemistry.



J. Sabine Becker

Dr habil. J. Sabine Becker is head of the BrainMet (Bioimaging of Metals in Brain and Metallomics) laboratory at the Central Division of Analytical Chemistry, Research Centre Juelich, Germany. Her present research activities are focused on development and application of advanced BrainMet techniques by LA-ICPMS. She has pioneered imaging LA-ICP-MS for quantitative micro- and nanolocal analysis of metals for brain research

*combined to metallomics. She is the author of 313 scientific publications, the handbook of "Inorganic Mass Spectrometry" Wiley, 2007 and is a member of several Advisory Boards *e.g.*, of the Int. J. Mass Spectrom., J. Anal. At. Spectrom. and Talanta.*

Table 1 Overview of metals and other elements mentioned in this manuscript

Element	Symbol	Atomic mass	Stable isotopes ^a	Function mentioned in this manuscript
Argon	Ar	39.95	³⁶ Ar, ³⁸ Ar, ⁴⁰ Ar	Primary ion beam of SIMS; a carrier gas in ICP-MS
Bismuth	Bi	208.98	²⁰⁹ Bi	Primary ion beam of SIMS
Boron	B	10.81	¹⁰ B, ¹¹ B	Boron neutron capture therapy; boron distribution in cell
Bromine	Br	79.90	⁷⁹ Br, ⁸¹ Br	Bromine distribution in tissue
Calcium	Ca	40.08	⁴⁰ Ca, ⁴² Ca, ⁴³ Ca, ⁴⁴ Ca, ⁴⁶ Ca, ⁴⁸ Ca	Calcium distribution in cell and tissue
Caesium	Cs	132.91	¹³³ Cs	Carbon ¹² C, ¹³ C Primary ion beam of SIMS
Copper	Cu	63.55	⁶³ Cu, ⁶⁵ Cu	Primary ion beam of SIMS
Gallium	Ga	69.72	⁶⁹ Ga, ⁷¹ Ga	Copper distribution in cell and tissue
Gold	Au	196.97	¹⁹⁷ Au	Primary ion beam of SIMS
Iron	Fe	55.85	⁵⁴ Fe, ⁵⁶ Fe, ⁵⁷ Fe, ⁵⁸ Fe	Primary ion beam of SIMS; Au plates used for embedding biological sample
Lithium	Li	6.94	⁶ Li, ⁷ Li	Iron distribution in cell and tissue
Manganese	Mn	54.94	⁵⁵ Mn	Generated from boron nuclear reaction in biological tissue
Oxygen	O	16.00	¹⁶ O, ¹⁷ O, ¹⁸ O	Manganese distribution in cell and tissue
Phosphorus	P	30.97	³¹ P	Primary ion beam of SIMS
Potassium	K	39.10	³⁹ K, ⁴¹ K	Phosphorus distribution in cell and tissue
Selenium	Se	78.96	⁷⁴ Se, ⁷⁶ Se, ⁷⁷ Se, ⁷⁸ Se, ⁸⁰ Se, ⁸² Se	Potassium distribution in cell and tissue
Silicon	Si	28.09	²⁸ Si, ²⁹ Si, ³⁰ Si	Selenium distribution in cell and tissue
Silver	Ag	107.87	¹⁰⁷ Ag, ¹⁰⁹ Ag	Silicon plates used for embedding biological sample
Sodium	Na	22.99	²³ Na	Silver needle used to defocused laser beam in nano-LA-ICP-MS
Sulfur	S	32.07	³² S, ³³ S, ³⁴ S, ³⁶ S	Sodium distribution in cell and tissue
Zinc	Zn	65.39	⁶⁴ Zn, ⁶⁶ Zn, ⁶⁷ Zn, ⁶⁸ Zn, ⁷⁰ Zn	Sulfur distribution in cell and tissue
				Zinc distribution in cell and tissue

^a Based on the Berkeley Laboratory Isotopes Project.

pathophysiology may result, when metallomics studies are guided by the spatial information provided by bioimaging techniques. Of interest are the organization and dynamics of metals and metal-containing biomolecules at the cellular and tissue levels, especially in the study of human samples at different stages of disease, and in animal models with and

without experimental therapies targeting the metabolism of selected metals or the introduction of the metals themselves.

This review is not intended to be a comprehensive literature review of various imaging techniques. Instead, it is written primarily as a commentary guide and even a tutorial to the application of three advanced metallomics techniques SXRF,

Table 2 Comparison of the three common metal imaging techniques

	SIMS			LA-ICP-MS
	Standard	NanoSIMS	SXRF	
Sample material	Semi-thin or thin sections of epoxide-embedded material, vacuum compatible		Hydrated, dried, or embedded material. Vacuum not obligatory	Native 10–40 μm cryo-sections, laser ablated at atmospheric pressure
Field of view	few mm ²	0.1 mm ²	Sub mm ² to cm ²	0.01–200 cm ²
Spatial resolution	0.1–10 μm	> 50 nm	> 150 nm	5–200 μm
Penetration depth	1–10 nm		100–1000 μm	ablation of the section thickness
Mass range/u	Standard: 10–500 MeSIMS: –1500	10–250	12–250	6–250
Detection limit/ g g ⁻¹	at 10 μm spot diam.	50 nm spot diam.	2 × 15 μm ² spot ^a	100 μm laser beam
	Na 10 ⁻¹⁰	10 ^{-2f}	—	10 ⁻⁷
	P 10 ⁻⁸		10 ^{-4a} , 10 ^{-5b}	10 ⁻⁷
	Fe		10 ^{-7a} , 10 ^{-5b} , < 10 ^{-7c}	10 ⁻⁷
	Cu 10 ^{-8e}	10 ^{-2f}	10 ^{-7a}	10 ⁻⁸
	Zn 10 ⁻⁷	10 ^{-2f}	10 ^{-7a}	10 ⁻⁷
Dynamic range	10 ⁵	10 ^{2f}	10 ^{3d}	> 10 ⁹
Number of elements		5–7 (multicollector SIMS)	Practically ≈ 20	40 (quadrupole ICP-MS)
Additional detection capability	Isotopes; biomolecules (< 2000 Da); quantitative imaging, but difficult due to matrix effect		Oxidative states; non-destructive; quantitative imaging	Isotopes; quantitative imaging

Note that parameters significantly vary for each individual application. Values from typical settings are given for rough orientation only. Data adapted from Becker, Inorganic mass spectrometry 2007 and EAG AN339,^a Somogyi *et al.*, 2001 at the ESRF ID18F beamline, a highly stable end station dedicated to quantitation.^{43 b} Cotte *et al.*, 2007 at the ESRF ID21 beamline, 0.4 × 1 μm² spot.^{44 c} Ortega *et al.*, 2007 at the ESRF ID22 beamline at 100 nm spot diameter (0.05 ng cm⁻²; the area mass of cell being 100 μg cm⁻²).^{13a d} The dynamical range of XRF largely depends on the element composition in the sample due to spectral overlap specially of elements with neighboring *z* number. ^e Sykes *et al.*, 1994.^{45 f} CAMECA product brochure.

SIMS, and LA-ICP-MS. Table 1 provides a quick overview of metals and other elements mentioned in this manuscript. Table 2 compares the basic operational parameters of these techniques. Among these parameters, the sample material and the penetration depth will help us to choose the most suitable technique for sampling. Field of view, spatial resolution, mass range, detection limit, dynamic range, the number of simultaneous masses or elements, and the capability to identify isotopes and oxidative states will help us to understand the advantages and limitations of each technique. Moreover, the reader requiring further information regarding instrumentation and measurement procedures (such as the development and production of biological samples, data acquisition and calibration protocols) is directed to several excellent reviews, such as those of Fahrni⁸ (SXRF), Boxer *et al.*⁹ (SIMS), and Becker *et al.*¹⁰ (LA-ICP-MS). Moreover, a very recent exhaustive review in metal bioimaging from Fahrni group is highly recommended.¹¹

Techniques commonly used in bioimaging of metals

SXRF microscopy uses an X-ray beam to excite the inner shell electrons and, ultimately, to generate measurable X-ray fluorescence. Each element has a unique fluorescence spectrum, so this technique allows for multi-element analysis. Another advantage of using SXRF is that the sample is not damaged during the measurements. SXRF provides qualitative and quantitative information on the topography, concentration and oxidative state of metal cations¹² (see Table 2 for the basic characteristics of SXRF). SXRF instruments with micrometre or higher resolution are available at several synchrotron sources, such as the Advanced Photon Source (Argonne National Laboratory, Argonne, USA; www.aps.anl.gov), the European Synchrotron Radiation Facility (Grenoble, France; www.esrf.eu), and the SPring-8 Facility (Hyogo, Japan; www.spring8.or.jp/en/). For instance, an SXRF nanoprobe (nano-SXRF) was developed at the European Synchrotron Radiation Facility, which has a 90 nm X-ray beam.¹³

In addition to SXRF, X-ray based imaging techniques also include bench-top X-ray fluorescence analysis (XRF), proton or particle induced X-ray emission (PIXE), electron probe X-ray microanalysis (EPXMA) or scanning- or transmission electron microscopy energy dispersive X-ray analysis (SEM-EDS or TEM-EDS). Among these techniques, SXRF has the highest element sensitivity due to absence of a bremsstrahlung background, while EPXMA provides the highest spatial resolution on very thin samples. Bench-top micro-XRF is commercially available, integrating mapping capacities at 30 μm spatial resolution and detection limits at approximately 10–100 ppm (Model SEA5120A, SII NanoTechnology Inc., Tokyo, Japan, www.siint.com). There are two other bench-top micro-XRF systems, one is commercialized by Horiba Jobin-Yvon (Japan) and the other one by EDAX (USA). SEM-EDS or TEM-EDS platforms are also commercially available (*e.g.*, Bruker QUANTAXTM and Zeiss AURIGATM).

SIMS is a sensitive surface analytical mass spectrometric technique for imaging of elements, isotopes or molecules, and depth profiling and trace analysis. This can be used, for example, for the determination of contamination and element

distribution on solid sample surfaces, such as biological surfaces or tissue sections. In SIMS, the components of the solid sample surface are sputtered during bombardment with a focused primary ion beam [*e.g.*, argon (Ar), caesium (Cs), gallium (Ga), oxygen (O), gold (Au), or bismuth (Bi) cluster ions (Table 1)] of sufficiently high ion energy (from 0.2–40 keV) in a high-vacuum ion source.¹⁴ The positively or negatively charged secondary ions generated during the sputtering process are extracted into a double focusing sector field, quadrupole-based or time-of-flight (ToF) mass spectrometer with single ion detection. ToF-SIMS (*e.g.*, ION-TOF, Münster, Germany) is equipped with three primary ion sources for sputtering of sample surface, and has a higher transmission of ions and a broader mass-to-charge range than sector field SIMS. Table 2 introduces the basic characteristics of SIMS.

Nano-SIMS, using a double focusing sector field mass spectrometer, allows cellular imaging techniques to reach high spatial resolution at the nanometre scale (*e.g.*, 50 nm using Cs primary ions or 150 nm using O primary ions). This technique was first reported by Slodzian *et al.* in 1992.¹⁵ SIMS instruments, Nano-SIMS 50 and 50 L from CAMECA Instruments (Cameca, Courbevoie, France) are currently on the market and are valuable imaging instruments in the biosciences with nanometre resolution.¹⁶ Nano-SIMS is equipped with multiple ion collectors for isotope analysis and can analyze different isotopes simultaneously (see Table 2). In general, SIMS can be performed on semi-thin (300–500 nm) or thin (60–80 nm) sections of fixed, dehydrated and embedded materials (electron microscope preparations) set on clean silicon (Si), stainless steel, or Au plates. SIMS can also be applied to native tissue mounted onto conventional glass slides using charge compensation. SIMS using Bi, Au, or carbon (C) cluster ion bombardment having spatial resolutions of a few micrometres and below have been applied to an increasing extent for biomedical applications, especially for analyzing relatively small biomolecules (<1000 Da) in cells and tissues.¹⁷

LA-ICP-MS uses a finely focused laser beam with micrometre spot size to ablate a biological sample. The ablated material is transported into the inductively coupled plasma (ICP) source of the mass spectrometer using a carrier gas (Ar). In the ICP, the ablated material is vaporized, atomized and ionized. The formed ions are extracted into the mass spectrometer and separated according to their mass-to-charge ratio. Table 2 describes the basic characteristics of LA-ICP-MS. Commercial laser ablation systems for sample introduction include UP 213 or UP 266 (New Wave Research, Fremont, CA),¹⁸ and LSX 213, 200 or 500 (CETAC Technologies, Omaha NE, USA¹⁹) instruments, whereas quadrupole-based and sector field ICP mass spectrometers are commercially available from Thermo Fisher Scientific (Bremen, Germany), Agilent Technologies (Santa Clara, CA, USA), and Perkin Elmer Sciex (Toronto, Canada). LA-ICP-MS has been established as a sensitive mass spectrometric technique for the bioimaging of metals, metalloids, and nonmetals at trace levels in microtome sections of biological tissues. The optimum thickness of the specimen, in this case, is 20–30 μm .²⁰ In LA-ICP-MS (under dry plasma conditions)

interference problems are decreased compared to the use of solution nebulization ICP-MS (under wet plasma conditions). To quantify LA-ICP-MS data, reliable quantification strategies such as the use of homogeneous matrix-matched laboratory standards or solution-based calibration in bioimaging of metals in tissues have been established.^{19,21} LA-ICP-MS has a multi-element capability (see Table 2) and can provide quantitative specific metal distribution in thin tissue sections of human or rodent brain.^{21,22} In addition, LA-ICP-MS instrumentation is significantly more economical and easy to handle than the other two techniques. Advanced quantitative bioimaging techniques are employed in the BrainMet (Bioimaging of Metals in Brain and Metallomics; www.brainmet.de) laboratory for quantitative routine measurements on diseased and healthy brain sections with spatial resolutions of 5 to 150 μm .²³

Nano-LA-ICP-MS has recently been initiated to improve the lateral resolution of LA-ICP-MS to the nanometre resolution.²⁴ The basic principle behind this innovation is to insert a thin silver (Ag) needle into a defocused laser beam using the near-field effect in laser ablation. The tip of the thin needle acts as a magnifier. Thus, the focusing of photons is 300 times better than the best focusing lens and presents a strong field enhancement. Becker *et al.*²⁵ have established the electrochemical etching of appropriate, very sharp Ag tips and provided the first demonstration of the instrumentation in elemental and isotopic analysis, while ablating and analyzing nanometre scale spots in biological samples. Very recently, a novel breakthrough of scaling down the bioimaging of metals

by the coupling of a laser microdissection apparatus to an inductively coupled plasma mass spectrometry (LMD-ICP-MS) instrument has been obtained.²⁶ LMD-ICP-MS holds great potential for medical and biological investigations on small-size samples, such as single cells.

Bioimaging of metals at the single-cell level

Improvements in the design of SIMS and SXRF fulfil the requirements for mapping biological trace metals at sizes that are compatible with the analysis of most subcellular organelles, including mitochondrion, lysosome, and secretory vesicle. For example, SXRF can detect as little as 10^{-18} g of Fe within a cellular structure that has a diameter of only 90 nm.^{13a} Importantly, these techniques can detect the distribution of metal ions within the specific sample directly, without changing the natural charged states of the components of interest.

Until now, most imaging studies have focused on the distribution studies of Fe in single cells, and, in particular, on the association between Fe content and the pathogenesis of neurodegenerative diseases. For example, Fe accumulates in the brain of patients with Parkinson's disease. This has been proposed as a mechanism that contributes to the selective loss of dopaminergic neurons during progression of the disease. In addition, dopamine can form stable complexes with Fe *in vitro*.²⁷ Thus, it is reasonable to propose that Fe accumulates in dopamine neurovesicles. Using SXRF microscopy at 90 nm spatial resolution, Ortega and coworkers have provided convincing data corroborating this hypothesis.^{13a} To prepare samples for

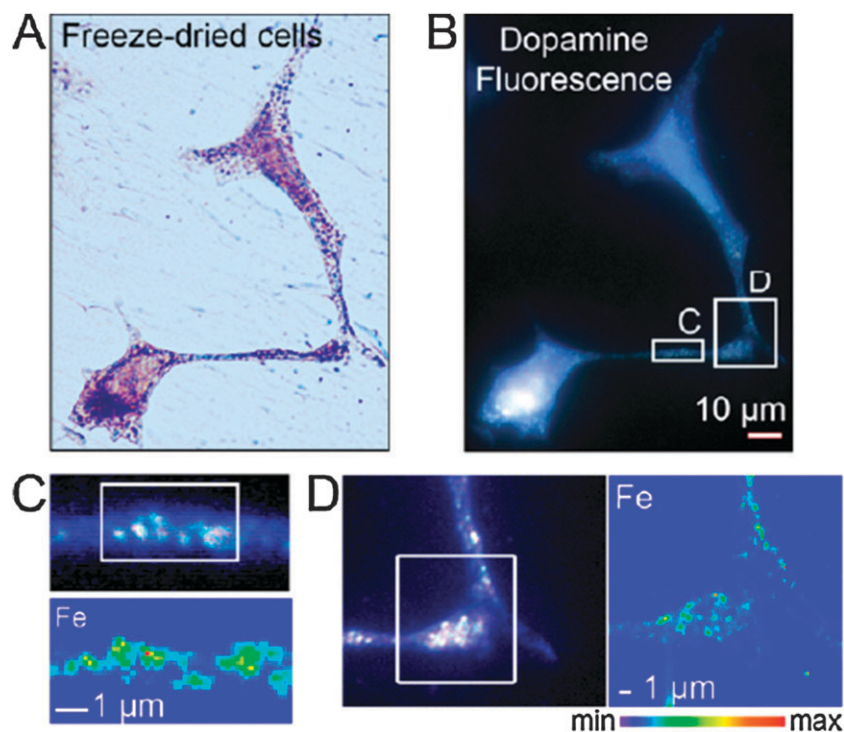


Fig. 1 Nano-SXRF reveals the location of Fe within dopamine neurovesicles. Visible light microscopy of freeze-dried cells (A) and fluorescence microscopy of the same freeze-dried cells (B) allow the distribution of dopamine to be determined. Panels C and D compare the same region imaged using fluorescence to visualize dopamine and using nano-SXRF to localize the Fe. This study indicates that dopamine and Fe colocalize within 200 nm structures that are characteristic of dopamine neurovesicles, as identified using fluorescence microscopy. The integration time per scan point was varied from 300 ms to 1 s. The min-max range bar units are arbitrary. Reproduced from Ortega *et al.*, PLoS One, 2007.^{13a}

SXRF study, cells were rinsed with phosphate buffer solution, cryofixed at $-160\text{ }^{\circ}\text{C}$ by plunge freezing into isopentane chilled with liquid nitrogen, and freeze dried at $-35\text{ }^{\circ}\text{C}$. Fig. 1C and D show that the distribution of dopamine detected by the fluorescence microscopy is co-localized with Fe particles detected by nano-SXRF. Furthermore, the authors find that the inhibition of dopamine synthesis results in a decreased vesicular storage of Fe. This appears the first direct evidence to support the concept that dopamine-Fe complexes may exist in dopaminergic neurons. This study also reported some interesting discoveries relating to the subcellular topography of Fe and Zn. First, whether treated with excess Fe or not, the cells show the same subcellular topography of Fe. Second, Fe-rich structures are found in the cytosol, in neurite outgrowths, and at the distal ends of dopamine-producing PC12 cells. However, K and Zn are not selectively distributed to dopamine neurovesicles, contrary to observation made in relation to the topography of Fe. Third, Zn has slightly elevated levels in the nucleus. Note that Zn functions as a cofactor in the Zn-finger transcription factors in the nucleus.²⁸

In addition to SXRF, the metal subcellular distribution also has been studied using SIMS. Boron (B) is a trivalent metalloid, an essential plant nutrient and a component of boromycin—an antibiotic compound produced by *Streptomyces*. This element has been used for drug design²⁹ and boron neutron capture therapy (BNCT) for cancers, such as glioblastoma multiforme.³⁰ Glioblastoma multiforme is the most common and aggressive type of primary brain tumors in humans. Boron has two stable non-radioactive isotopes in nature, ^{10}B and ^{11}B . When ^{10}B is irradiated with low-energy thermal neutrons, a nuclear reaction occurs that yields high linear energy transfer α particles and recoils ^7Li (lithium) nuclei. The impact of this reaction is limited to $8\text{ }\mu\text{m}$ in tissue, equal to or less than one cell diameter. BNCT has been designed utilizing the principle of this neutron capture reaction. To better understand the biological consequence of BNCT, it is necessary to study the subcellular distribution of boron in biological samples. Using SIMS isotope images with a 500 nm spatial resolution, Fig. 2 illustrates one study by Chandra and colleagues to image ^{12}C , ^{39}K , ^{23}Na , ^{40}Ca , and ^{10}B distribution in human glioblastoma T98G cells treated with a BNCT agent, *p*-boronophenylalanine (BPA).³¹ One particular sample preparation (*i.e.*, cryogenic sandwich-fracture method) is also elegantly described in this article. This method has great potential to apply for the sample preparation with other metallomics techniques. Fig. 2a shows an optical image of several fractured, freeze-dried cells. The boundaries of the nuclei are labeled by a dotted line in two cells, and the mitochondria-rich perinuclear cytoplasmic region is indicated using arrows. Fig. 2e shows lower concentrations of ^{40}Ca in the nucleus *versus* the cytoplasm. Fig. 2f shows a distinctly lower concentration of ^{10}B in the mitochondria-rich perinuclear cytoplasmic regions (*cf.* arrows), whereas there is no discernible difference in the localization of ^{10}B between the nucleus and the remaining cytoplasm in T98G interphase cells. By the way of contrast, in another experiment, the BPA-treated T98G metaphase cells reveal significantly lower concentration of ^{10}B in their chromosomes than in their cytoplasm. The cell cycle can be divided into two periods: interphase and mitosis. Mitosis can be further divided

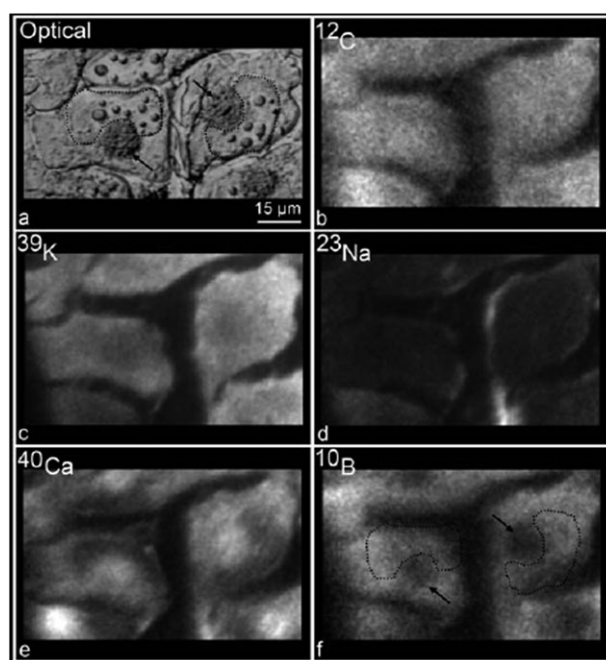


Fig. 2 Subcellular metal distribution in interphase T98G human glioblastoma cells using SIMS. Interphase T98G human glioblastoma cells were treated with $110\text{ }\mu\text{g mL}^{-1}$ BPA for 1 h. In the reflected light Nomarski image (a), the boundaries of the nucleus of two fractured freeze-dried cells are shown with dotted lines. The mitochondria-rich perinuclear cytoplasmic regions are shown by arrows in two cells. A SIMS analysis of the same cells revealing the subcellular isotopic distributions of ^{12}C (b), ^{39}K (c), ^{23}Na (d), ^{40}Ca (e) and ^{10}B (f) is shown. The areas within the dotted lines show the position of the nuclei, and arrows indicate the organelle-rich perinuclear cytoplasmic region in SIMS images. The image integration time of the CCD camera for the ^{39}K and ^{23}Na images was 0.4 s . The ^{12}C , ^{40}Ca and ^{10}B images were integrated for 2 min each. Reproduced with permission from Wiley, 2008.³¹

into following sequential phases: prophase, metaphase, anaphase, telophase and cytokinesis. The exciting finding suggests the heterogeneity of B distribution in different cell cycle phases (interphase *versus* metaphase). Overall, these studies demonstrate that the metal bioimaging detected by SXRF and SIMS provides a novel perspective to investigate the cellular events at physiological and pathophysiological levels.

Bioimaging of metals at the organ and tissue levels

Conventional analytical techniques, such as ICP-MS and atomic absorption spectrometry,³² examine the total metal ion content after homogenization and digestion of the biological tissues or organs. However, these techniques do not provide sufficient information on the spatial distribution of metal ions. Therefore imaging studies are important because many metal ions (*i.e.*, Cu, Fe, Zn, Mn, and Ca) are dispersed inhomogeneously in human tissues. Moreover, the biochemical reactions and physiological functions of metal cations are determined not only by their concentration, but also by their distribution within the tissues. Heretofore, histological or histochemical staining has been used to visualize the inhomogeneous distributions of selected metal cations (*e.g.*, Fe) within tissues.³³ However,

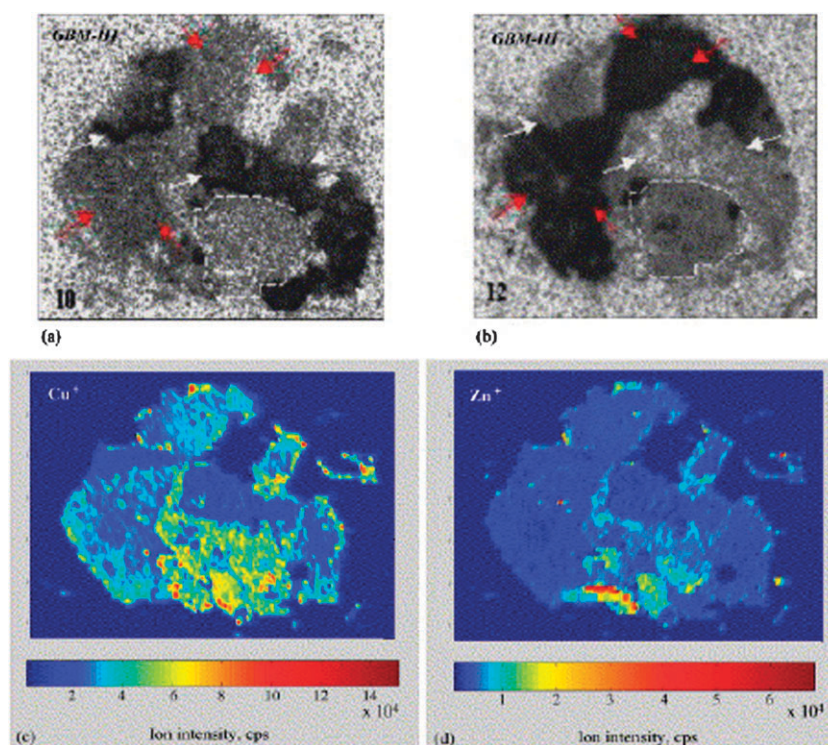


Fig. 3 LA-ICP-MS reveals the location of Cu and Zn on a slice of a human glioblastoma sample. Adjacent sections underwent receptor autoradiography using radioligands for peripheral benzodiazepine receptors (pBR), to define the area of the tumor (the black areas indicated by white arrows in panel a), and for A1 adenosine receptors (A1AR) to define the tumor invasion zone (the black areas indicated by red arrows in panel b). Areas of intratumoral hemorrhage are indicated by a dotted line (a and b). The sections containing the glioblastoma were entirely ablated line by line with LA-ICP-MS. Laser scan speed was $40 \mu\text{m s}^{-1}$. Laser beam diameter was $50 \mu\text{m}$. The areas of intratumoral hemorrhage showed the highest levels of Cu and Zn. The tumor invasion zone (high A1AR) and the cellular tumor mass region (high pBR) can be detected clearly using the LA-ICP-MS measurements. Both elements are completely lacking within the tumor (c and d). Reproduced with permission from Elsevier, 2006.³⁶

histological methods are relatively nonspecific, have a relatively higher background and allow only one element to be mapped per section. The quantification of images is also challenging. The introduction of novel imaging techniques with multi-element capability provides a valuable tool for overcoming these limitations.

A vivid example of the application of this technique at the tissue/organ level comes from studies into the role of Cu in neovascularization and cancer. Recent clinical studies have suggested that lowering Cu levels may be an effective antiangiogenic approach to cancer treatment and that this is, at least in

part, due to the regulation of neovascularization (see the review by Brewer³⁴). Indeed, neovascularization is known to be sensitive to the level of Cu.³⁵ However, relatively little is known about how Cu is distributed in cancerous tissues. Using LA-ICP-MS, Becker's group quantified the bioimages of metals, including Cu and Zn, in histological sections of specimens from patients with glioblastoma multiforme.³⁶ The black area shown in Fig. 3a indicates the area of the tumor. Surprisingly, there was very little Cu detected in the tumor (see Fig. 3c). In contrast, the black area shown in Fig. 3b indicates the area of the tumor invasion zone, showing that Cu accumulated in the area around

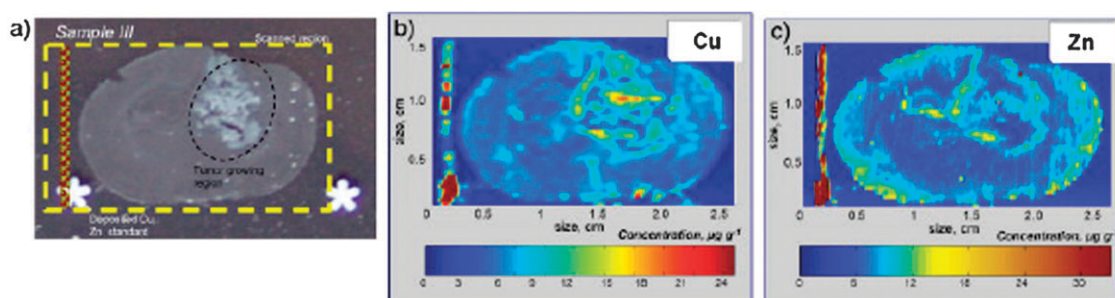


Fig. 4 LA-ICP-MS reveals the location of Cu and Zn in a cross section of a rat brain sample containing tumor tissue. The areas of tumor are indicated by black dotted lines (a). The images of Cu (b) and Zn (c) are measured by LA-ICP-MS. Scan speed of laser ablation was $40 \mu\text{m s}^{-1}$, laser beam diameter $50 \mu\text{m}$. Reproduced with the permission from Elsevier, 2008.^{22a}

the tumor (see Fig. 3c). This finding suggests that cell types other than tumor cells may be sensitive to Cu, *e.g.*, tumor-associated macrophages, which usually surround the tumor. Another possibility is that Cu may play different roles at different stages of the progression of the disease and in different types of tumor. The latter possibility was supported by another study performed by the same group. In that study, F-98 glioma cells (10^3) were implanted into the right caudate putamen of rat brain using stereotaxic guidance. To prepare the sample for LA-ICP-MS study, the brain was frozen in isopentyl alcohol at $-50\text{ }^\circ\text{C}$ and cut into $20\text{ }\mu\text{m}$ thick slices at $-16\text{ }^\circ\text{C}$ for further LA-ICP-MS.^{22a} The authors find that the tumor tissue (the right brain hemisphere) is more enriched in Cu and Zn than the control tissue (the left brain hemisphere) (see Fig. 4b). However, in one case, shortly after incubation with the tumor cells, the site of the tumor became visible through a small depletion of Cu. Although no mechanism has been discovered that can explain the apparently contradictory results between these human *versus* animal studies, nevertheless, these data indicate that the role of Cu in cancer and neovascularization is more complicated than the original assumption. Using metal imaging LA-ICP-MS, more animal model studies can be developed, and further clinical studies can be carried out to decipher this important medical puzzle.

An important morphological change in aging neurons is an accumulation of autophagic vacuoles occupied by neuromelanin, a dark pigment synthesized within specific catecholamine-producing neurons.³⁷ Fedorow *et al.* described three phases during the development of neuromelanin.³⁸ Briefly, in phase I (2–3 years of age), the dopaminergic neurons develop a faint and diffuse pigmentation; in phase II (childhood and adolescence; 3–20 years of age), the cellular volume filled with neuromelanin increases and becomes darker; and in phase III (middle and later life), sustained maturation of neuromelanin (pigment darkening) occurs without further cellular volumetric increase. To further the understanding of the cellular metallomics of neuromelanin, Bohic and colleagues studied intracellular metallic topography during human neuromelanin development using nano-SXRF.³⁹ Pigmented neurons can be clearly identified in the unstained paraffin sections (Fig. 5a). Fig. 5b illustrates an average metal spectrum from a region of interest ($\sim 15 \times 15\text{ }\mu\text{m}^2$) within mature (phase III) neuromelanin containing cells (in a 94 year old male). The elements specifically distributed within the neuromelanin include S, Ca, Fe, Cu, Zn, and Se (Fig. 5c). P is homogeneously topographic throughout the cytoplasm and nucleus, whereas Mn presents a faint and heterogeneous topography within the neuromelanin (Fig. 5c). In additional studies, microdomains of various elements are observed within the neuromelanin. These irregular microdomains of micrometre or submicrometre size are most apparent at phase III of pigment development (aging). The authors further hypothesize that metal-rich binding domains in neuromelanin represent physiologically active structures that have developed as a functional adaptation to efficiently bind potentially toxic metals without the cell being overloaded with pigment. Moreover, the dynamic changes in the levels of Ca, Fe, and Cu revealed in this study enrich our knowledge about the use of metallomics

in aging. Ca concentration within brain tissue (substantia nigra) is highest during prenatal development, prior to the development of neuromelanin. Following development of the pigment, the level of Ca gradually increased in the neuromelanin from early childhood (3 years old, phase I) to adolescence (15 years old, phase II), but declined during later life. Neuromelanin-associated Fe steadily and significantly increases with age; its level in the oldest subject (94 years old) is almost 12 times higher than that observed at 3 years of age. Cu content of neuromelanin also increases in early adulthood but decreases in the aged brain. The biological implication of the presence of metals in neuromelanin is also notably discussed by the authors. For example, Mn is detected only in the elderly and is inhomogeneously topographic throughout the neuromelanin. This might result from an elevated expression of manganese-SOD in response to enhanced oxidative stress. Another possibility is that it results from less effective mitochondria autophagocytosis in senescent neurons, resulting in the transfer of mitochondrial Mn to neuromelanin.³⁹

Suggestions and future directions

It is important to acknowledge that these metals imaging techniques are not without limitations. In general, the spatial resolution and sensitivity are negatively correlated. A smaller spot or beam size yields a reduced signal. In addition, none of the methods presented has a high throughput capability; all require a relatively long measuring time range. Care should be taken that metals of interest should be not washed out during the sample preparation. Formalin-fixed and paraffin-embedded tissue should be de-paraffinized prior to LA-ICP-MS, because paraffin can contaminate the ion source of the mass spectrometer. However, this preparation can be used directly for SXRF. In some studies, the lower concentrations of some metals such as Fe were measured using formalin-fixed and paraffin-embedded tissue.³⁹ This could have been due to leaching of the metals from the tissues into the formalin solution or following paraffin embedding. However, this effect should have been consistent in all tissues studied, because they are all fixed in formalin and further processed using a standardized protocol.³⁹ Frozen processed samples are acceptable for all three metallomics techniques mentioned in this article, and this method theoretically protects the native state of the tissue *in vivo* (particularly with respect to the preservation of diffusible ions). However, such samples are more difficult to prepare and transport. Moreover, SIMS, SXRF and LA-ICP-MS cannot analyze live cells up to now. As a complementary approach, membrane-diffusible fluorescent probes can overcome this limitation to examine the subcellular availability of transition metal cations, such as Zn⁴⁰ or Cu.⁴¹ However, little is known about whether such probes can attach covalently to important functional groups, thereby introducing unnatural charges into cells. And the metal specificity/selectivity of fluorescence probe toward one particular metal is not that of element based mass spectrometry. Therefore, it is important to carefully consider the pros and cons of each method during experimental design.

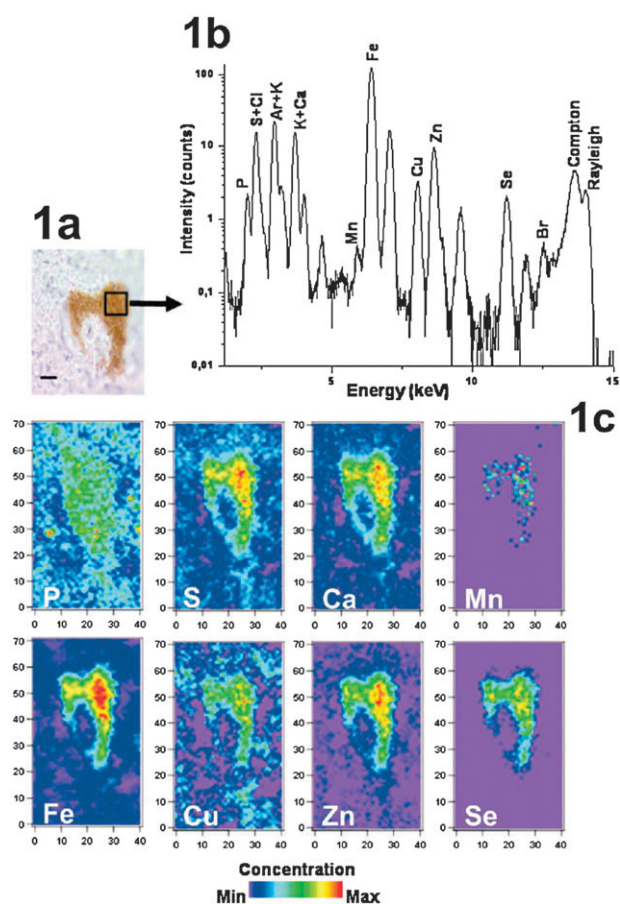


Fig. 5 Metallic topography within neuromelanin using Nano-SXRF. (a) Optical micrograph of a neuromelanin-containing dopaminergic neuron from an 8 μm human substantia nigra pars compacta tissue section (from a 94 year old patient). The scale bar represents 10 μm . (b) A typical averaged spectrum extracted from an intracellular region of interest (the black square on the optical micrograph) containing neuromelanin (arrow). The display uses a log scale for the average number of counts collected over the neuromelanin region. The K α X-ray emission lines corresponding to phosphorus (P), sulfur (S), and K overlapping with Ca, Mn, Fe, Cu, Zn, selenium (Se), and bromine (Br) are reported, as well as the contribution of the inelastic (Compton) and elastic (Rayleigh) X-ray scattering processes. (c) The corresponding elemental 2D maps are presented and represent a scanning area of 80 μm \times 70 μm (horizontal \times vertical). Dwell time was in the 100 ms to 1 s range. The minimum (Min) and maximum (Max) of the color bar are for P (0–1.77%), S (0.1–2.32%), Ca (40–1060 ppm), Mn (0–6.2 ppm), Fe (12–804 ppm), Cu (0–18.2), Zn (0–59 ppm), and Se (0–5.3 ppm). Reproduced with permission from ACS publication, 2007.³⁹

Nevertheless, recent publications demonstrate that the sensitivity, spatial resolution, specificity, and quantification of bioimaging of metals are suitable for biomedical research. However, most of these publications focus on the physiopathological mechanisms of neurological diseases. Relatively few studies have been performed using other disease models such as cardiovascular disease. As a useful attempt, we recently applied LA-ICP-MS technique to determine and quantify the metal distribution in mouse heart.⁴² In the future, it will be important to apply these powerful techniques to further investigate the metal distribution in various human diseases.

Abbreviations

BNCT	boron neutron capture therapy
BPA	<i>p</i> -boronophenylalanine
EPXMA	electron probe X-ray microanalysis
ICP	inductively coupled plasma
LA-ICP-MS	laser ablation inductively coupled plasma mass spectrometry
LMD-ICP-MS	laser microdissection inductively coupled plasma mass spectrometry
PIXE	proton or particle induced X-ray emission
SEM-EDS	scanning electron microscopy energy dispersive X-ray analysis
SIMS	secondary ion mass spectrometry
SXRF	synchrotron X-ray fluorescence
TEM-EDS	transmission electron microscopy energy dispersive X-ray analysis
ToF	time-of-flight
XRF	X-ray fluorescence analysis

Acknowledgements

This work was supported by an AHA National Scientist Development Grant (0835268N).

References

- W. P. Blackstock and M. P. Weir, *Trends in Biotechnology*, 1999, **17**, 121.
- A. C. Rosenzweig, *Chemistry & Biology*, 2002, **9**, 673.
- W. Mertz, *Science*, 1981, **213**, 1332.
- (a) S. G. Kaler, C. S. Holmes, D. S. Goldstein, J. Tang, S. C. Godwin, A. Donsante, C. J. Liew, S. Sato and N. Patronas, *The New England Journal of Medicine*, 2008, **358**, 605; (b) L. Poulsen, L. B. Moller, K. Plunkett, J. Belmont, Z. Tumer and N. Horn, *Genetic Testing*, 2004, **8**, 286.
- (a) Z. Qin, M. C. Gongora, K. Ozumi, S. Itoh, K. Akram, M. Ushio-Fukai, D. G. Harrison and T. Fukai, *Hypertension*, 2008, **52**, 945; (b) Z. Qin, S. Itoh, V. Jeney, M. Ushio-Fukai and T. Fukai, *Faseb J*, 2006, **20**, 334; (c) S. E. Afton, J. A. Caruso, B. E. Britigan and Z. Qin, *Biometals*, 2009, **22**, 531.
- R. Lobinski, J. S. Becker, H. Haraguchi and B. Sarkar, *Pure and Appl. Chem*, 2010, **82**, 493.
- R. N. Easter, Q. Chan, B. Lai, E. L. Ritman, J. A. Caruso and Z. Qin, *Vascular medicine (London, England)*, 2010, **15**, 61.
- C. J. Fahrni, *Current Opinion in Chemical Biology*, 2007, **11**, 121.
- S. G. Boxer, M. L. Kraft and P. K. Weber, *Annual Review of Biophysics*, 2009, **38**, 53.
- (a) J. S. Becker, M. Zoriy, A. Matusch, B. Wu, D. Salber, C. Palm and J. S. Becker, *Mass Spectrometry Reviews*, 2009; (b) J. S. Becker and N. Jakubowski, *Chemical Society Reviews*, 2009, **38**, 1969.
- R. McRae, P. Bagchi, S. Sumalekshmy and C. J. Fahrni, *Chem. Rev.*, 2009, **109**, 4780.
- (a) T. Paunesku, S. Vogt, J. Maser, B. Lai and G. Woloschak, *Journal of Cellular Biochemistry*, 2006, **99**, 1489; (b) C. T. Dillon, P. A. Lay, B. J. Kennedy, A. P. Stampfl, Z. Cai, P. Ilinski, W. Rodrigues, D. G. Legnini, B. Lai and J. Maser, *J. Biol. Inorg. Chem.*, 2002, **7**, 640; (c) T. Bacquart, G. Deves, A. Carmona, R. Tucoulou, S. Bohic and R. Ortega, *Analytical Chemistry*, 2007, **79**, 7353.
- (a) R. Ortega, P. Cloetens, G. Deves, A. Carmona and S. Bohic, *PLoS one*, 2007, **2**, e925; (b) A. Carmona, P. Cloetens, G. Deves, S. Bohic and R. Ortega, *J. Anal. Atom Spectrom.*, 2008, **23**, 1083.
- J. S. Becker, *Inorganic Mass Spectrometry, Principles and Applications*, Wiley, 2007.
- G. Slodzian, B. Daigne, F. Girard, F. Boust and F. Hillion, *Biology of the cell/under the auspices of the European Cell Biology Organization*, 1992, **74**, 43.

- 16 (a) J. L. Guerquin-Kern, F. Hillion, J. C. Madelmont, P. Labarre, J. Papon and A. Croisy, *Biomedical Engineering Online*, 2004, **3**, 10; (b) J. L. Guerquin-Kern, T. D. Wu, C. Quintana and A. Croisy, *Biochimica et biophysica Acta*, 2005, **1724**, 228.
- 17 T. G. Lee, J. W. Parka, H. K. Shona, D. W. Moon, W. W. Choib, K. Lib and J. H. Chung, *Appl. Surf. Sci.*, 2008, **255**, 1241.
- 18 J. Seuma, J. Bunch, A. Cox, C. McLeod, J. Bell and C. Murray, *Proteomics*, 2008, **8**, 3775.
- 19 J. S. Becker, M. V. Zoriy, C. Pickhardt, N. Palomero-Gallagher and K. Zilles, *Analytical Chemistry*, 2005, **77**, 3208.
- 20 J. S. Becker, *Int. J. Mass Spectrom.*, 2010, **289**, 65.
- 21 J. Dobrowolska, M. Dehnhardt, A. Matusch, M. Zoriy, N. Palomero-Gallagher, P. Koscielniak, K. Zilles and J. S. Becker, *Talanta*, 2008, **74**, 717.
- 22 (a) M. V. Zoriy, M. Dehnhardt, A. Matusch and J. S. Becker, *Spectrochimica Acta Part B: Atomic Spectroscopy*, 2008, **63**, 375; (b) M. Dehnhardt, M. V. Zoriy, Z. Khan, G. Reifenberger, T. J. Ekstrom, J. Sabine Becker, K. Zilles and A. Bauer, *J. Trace Elem. Med. Biol.*, 2008, **22**, 17.
- 23 J. S. Becker and D. Salber, *Trends in Analytical Chemistry*, 2010, **29**, 966.
- 24 (a) M. V. Zoriy, D. Mayer and J. S. Becker, *Journal of the American Society for Mass Spectrometry*, 2009, **20**, 883; (b) J. S. Becker, A. Gorbunoff, M. Zoriy, A. Izmer and M. Kayser, *J. Anal. At. Spectrom.*, 2006, **21**, 19.
- 25 J. S. Becker, M. Kayser, A. Gorbunoff, W. Pompe, G. Roedel, U. Krause-Buchholz and M. Przybylski, *German Patent* 2008.
- 26 J. S. Becker, S. Niehren, A. Matusch, B. Wu, H.-F. Hsieh, U. Kumbatim, M. Hamester, A. Plaschke-Schlütter and D. Salber, *Int. J. Mass Spectrom.*, 2010, **294**, 1–6.
- 27 I. Paris, P. Martinez-Alvarado, S. Cardenas, C. Perez-Pastene, R. Graumann, P. Fuentes, C. Olea-Azar, P. Caviedes and J. Segura-Aguilar, *Chemical Research in Toxicology*, 2005, **18**, 415.
- 28 D. J. Eide, *Biochimica et biophysica acta*, 2006, **1763**, 711.
- 29 P. Hunter, *EMBO Rep*, 2009, **10**, 125.
- 30 T. Yamamoto, K. Nakai and A. Matsumura, *Cancer Lett.*, 2008, **262**, 143.
- 31 S. Chandra, W. Tjarks, D. R. Lorey, 2nd and R. F. Barth, *Journal of Microscopy*, 2008, **229**, 92.
- 32 J. S. Becker, *Trends in Anal. Chem.*, 2005, **24**, 243.
- 33 J. R. Connor, G. Pavlick, D. Karli, S. L. Menzies and C. Palmer, *The Journal of Comparative Neurology*, 1995, **355**, 111.
- 34 G. J. Brewer, *Drug Discovery Today*, 2005, **10**, 1103.
- 35 (a) M. Ziche, J. Jones and P. M. Gullino, *Journal of the National Cancer Institute*, 1982, **69**, 475; (b) K. S. Raju, G. Alessandri, M. Ziche and P. M. Gullino, *Journal of the National Cancer Institute*, 1982, **69**, 1183.
- 36 M. V. Zoriy, M. Dehnhardt, G. Reifenberger, K. Zilles and J. S. Becker, *Int. J. Mass Spectrom.*, 2006, **257**, 27.
- 37 D. Sulzer, E. Mosharov, Z. Talloczy, F. A. Zucca, J. D. Simon and L. Zecca, *Journal of Neurochemistry*, 2008, **106**, 24.
- 38 H. Fedorow, G. M. Halliday, C. H. Rickert, M. Gerlach, P. Riederer and K. L. Double, *Neurobiology of Aging*, 2006, **27**, 506.
- 39 S. Bohic, K. Murphy, W. Paulus, P. Cloetens, M. Salome, J. Susini and K. Double, *Analytical Chemistry*, 2008, **80**, 9557.
- 40 K. Kikuchi, K. Komatsu and T. Nagano, *Current Opinion in Chemical Biology*, 2004, **8**, 182.
- 41 L. Zeng, E. W. Miller, A. Pralle, E. Y. Isacoff and C. J. Chang, *Journal of the American Chemical Society*, 2006, **128**, 10.
- 42 J. S. Becker, U. Breuer, H. F. Hsieh, T. Osterholt, U. Kumtabtim, B. Wu, A. Matusch, J. A. Caruso and Z. Qin, *Analytical Chemistry*, 2010.
- 43 A. Somogyi, M. Drakopoulos, L. Vincze, B. Vekemans, C. Camerani, K. Janssens, A. Snigirev and F. Adams, *X-Ray Spectrometry*, 2001, **30**, 242.
- 44 M. Cotte, E. Welcomme, V. A. Solé, M. Salomé, M. Menu, P. Walter and J. Susini, *Anal. Chem.*, 2007, **79**, 6988.
- 45 D. E. Sykes and A. Chew, *Surface and Interface Analysis*, 1994, **21**, 231.